Drug-Free Hybrid Nanoarchitecture Modulation of the Metastatic Behavior of Pancreatic Ductal Adenocarcinoma in Alternative *in Vivo* Models

Agata Zamborlin, Patrizia Sarogni, Valentina Frusca, Alessandra Gonnelli, Noemi Giannini, Maria Laura Ermini, Andrea Marranci, Francesca Pagliari, Chiara Maria Mazzanti, Joao Seco, and Valerio Voliani*
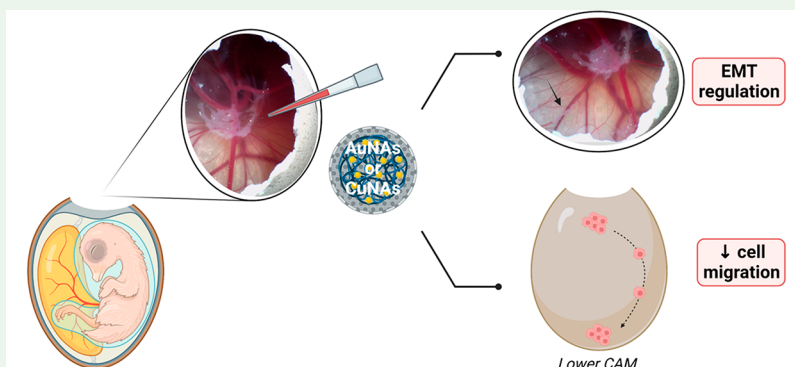
Cite This: https://doi.org/10.1021/acsanm.3c05299

Read Online

ACCESS | 📊 Metrics & More | 📰 Article Recommendations | 🆘 Supporting Information

Lower CAM

ABSTRACT: Metastasis is the key cause of treatment failure in most oncological patients. The spreading of cancer cells to distal tissues and organs can be associated with the epithelial-to-mesenchymal transition (EMT) that reduces or nullifies the effectiveness of the actual treatments. In this context, the establishment of effective antimetastatic agents is the final frontier in cancer research. Noble metal nanomaterials may allow advancements in this regard, but the issue of their persistence precludes their translation to clinics despite their antimetastatic properties. Here, we demonstrate that non-persistent gold and copper ultrasmall-in-nano architectures (NAs) conceived by a safe-by-design approach reduce tumor growth and modulate the progression of the metastasis by altering gene and protein expression of the EMT-related factors in alternative *in vivo* models of pancreatic ductal adenocarcinoma. Together with these findings, we also introduce an alternative biomodel for the evaluation of metastasis to mimic the heterogeneity of the metastatic phenomenon. On a broader basis, our results represent a promising step forward in the development of novel families of ultrasmall-in-nano antimetastatic agents for the establishment of the next clinical approaches for pancreatic cancer metastasis.

KEYWORDS: *Metastasis, nanoparticles, gold, copper, epithelial-to-mesenchymal transition, pancreatic carcinoma*

■ INTRODUCTION

Metastasis is considered the last stage in cancer development, it is associated with poor prognosis, and it accounts *per se* for the majority of relapses and deaths among oncological patients.[1,2] As one of the hallmarks of cancer, metastasis is defined as the spreading of cancer cells to distal tissues, eventually originating secondary tumors.[3] The acquisition of migratory properties is typically related to genome instability, which can itself result in the "epithelial-to-mesenchymal transition" (EMT). EMT is defined as the loss of epithelial features and the gaining of the mesenchymal ones.[2] At the molecular level, the expression of the epithelial protein E-cadherin is downregulated, whereas the mesenchymal proteins (e.g., Vimentin), matrix metalloproteinases (e.g., MMP9), and

EMT transcriptional factors (e.g., Snail and Twist) are overexpressed.[3] Due to its role in cancer cell spreading, EMT is a promising target for antimetastatic treatments.[4,5] Indeed, once EMT is reverted, it may be feasible to reduce recurrence by preventing the development of metastasis, reducing cancer invasion, and improving drug sensitivity.[6,7] Nevertheless, the involvement of EMT in several physiological

processes and its fine-tuning during cancer progression can cause massive side effects in patients. This is a critical aspect to consider and, regrettably, no definitive strategies to treat metastasis have yet been employed in clinical practice.[3] Furthermore, the spreading of cancer cells in the body and the latency in the development of visible new masses are obstacles to efficiently treat patients. For example, pancreatic ductal adenocarcinoma (PDAC) has a poor survival rate because of its silent development and spreading.[8] Therefore, even though PDAC has a modest incidence rate, it is one of the most lethal cancer types, with a 5-year survival below 10%.[9] The poor prognosis characterizing PDAC is mainly associated with the late diagnosis, which may be due to the lack of a screening program and specific symptoms.[8] Moreover, PDAC is highly metastatic, and the available treatments are mostly palliative.

Considering the issues in developing antimetastatic agents, nanostructured materials may have the potentiality to shift the paradigm for the treatment of metastasis, even if the field is still in its infancy.[10] Nevertheless, a tiny percentage of nano-products undergoing preclinical studies has reached the clinics.[3] The gap between nanoproducts in preclinical studies and clinics is likely ascribable to the difficulties in their clinical translation, as discussed by Germain et al.[11] Among the investigated nanoparticles, metal nanoparticles are attracting growing interest in the anticancer and antimetastatic treatment landscape. For instance, several AuNPs have demonstrated promising features as both drug carriers and active agents. For this reason, they have been intensely examined for theranostic purposes.[12] Moreover, as described by Zamborlin et al., several gold nanoparticles (AuNPs) have been recently investigated in vitro and in vivo for their antimetastatic potential. Overall, there is general consensus that AuNPs of different diameters reverted the EMT phenomenon, inhibiting cell proliferation and migration.[3] Unfortunately, metal persistence after the action is one of the main concerns for noble metal nanoparticle translation, which can be overcome by applying a safe-by-design approach based on the ultrasmall-in-nano strategy.[3,13] With a special focus on noninvasive and combined approaches, we developed the passion fruit-like nanoarchitectures (NAs) that comprise 1−3 nm ultrasmall metal nanoparticles (USMNPs) within a biodegradable silica nanocapsule.[14] Once the outer silica shell is biodegraded (24−48 h), USMNPs can be cleared from the organism avoiding the risk of metal persistence. Indeed, investigations on intravenous and intranasal administration of NAs indicate an efficient excretion of the metals without harming the major organs.[15−17] Remarkably, AuNAs have recently showed an antiangiogenic activity in in vivo chorioallantoic membrane (CAM) models of HPV-negative Head and Neck Squamous Cell Carcinoma (SCC-25) cells.[18] The correlation between angiogenesis and metastasis and the evidence reported by Arvizo et al. regarding the potential antiangiogenic and antimetastatic effects of AuNPs support the application of AuNAs as antimetastatic agents.[19] It is worth stressing here that the investigations on AuNPs as antimetastatic agents mainly involve nanoparticles bigger than the glomerular cutoff of kidneys, preventing any possible translation to the clinics.[3]

Among the metals investigated in oncological research, copper is gaining increasing interest. Copper is a trace element normally found in organisms, whose homeostasis is regulated in the gastrointestinal tract to avoid cell damage for excessive free copper ions.[20] Its role in cancer disease fluctuates between favoring the neoplasm's progression and outbreaking the homeostatic equilibrium.[21] For this reason, both Cu-chelating compounds and Cu-based complexes have been investigated for oncological purposes. In particular, several Cu complexes have been developed to affect DNA, topoisomerase I−II, proteasome, and cellular metabolism.[22] Some copper and copper oxide nanoparticles (CuNPs and CuONPs) have been explored as anticancer agents able to promote the production of reactive oxygen species (ROS) and the cascade of events that results in cell death.[23−25] Moreover, an antimetastatic effect of some CuNPs/CuONPs and copper complexes is also reported on various cancer lines.[21,26−32] Copper is more cytotoxic for cancerous than healthy cells, even though a detailed biological safety investigation is still lacking.[25] Indeed, it should be noted that copper ions released from CuNPs may interact with cysteine and methionine residues in proteins, potentially affecting their biological safety. On the other hand, rationally designed copper nanomaterials, such as copper nanoarchitectures (CuNAs), can be employed at therapeutic dosages to promote wound healing without inducing significant toxicity nor altering the systemic metabolism of copper.[33]

Here, we demonstrate that AuNAs modulate the metastatic behavior of PDAC in alternative in vivo models at non-toxic metal concentrations. We compared the findings with CuNAs to evaluate the dependence of the effects on the chemistry of the metal. Interestingly, both gold- and copper-based hybrid nanoarchitectures reduced tumor growth and metastasis progression, the latter after altering the gene and protein expression of EMT-related factors. These findings confirm the potentiality that hybrid nanoarchitectures may have for the establishment of novel clinical approaches in the treatment of pancreatic cancer metastasis. The assessments were performed by employing optimized alternative in vivo models of pancreatic carcinoma, the chorioallantoic membrane models (CAMs).[34] CAMs are alternative biomodels able to support tumor growth while respecting the 3Rs, in accordance with the European Parliament Directive 2010/63/EU. CAMs are suitable for metastasis investigation due to the high vascularization of the membrane.[35] Despite the poor vascularization characterizing PDAC, hematoxylin and eosin staining indicates an organized nest of tumor cells surrounded by stromal tissues and red blood cells in CAM tumor neovascularization.[36] The development of a stromal environment around the tumor is of particular interest, considering the role of the stroma in carcinogenesis and drug resistance. Therefore, compared to the other PDAC models, CAM reproduces the steps of both tumor and metastasis development in a shorter period of time in a naturally immunodeficient host, bridging the gap between in vitro and in vivo models.[36] Thanks to the employment of CAMs, we were able to time-dependently correlate the neoplasm's gene and protein expression with the quantified cancer cells migrated in the lower CAM and concomitantly monitor the primary tumor and the metastasis evolution in the upper CAM.

Overall, this work supports the establishment of the next clinical approaches for metastasis modulation by the employment of a family of antimetastatic ultrasmall-in-nano agents based on excretable metal nanomaterials. Furthermore, the introduction of a biomodel for advanced investigations regarding the metastatic behaviors of carcinomas especially impacts oncological and translational research by demonstrat-

ing the critical role CAMs play in the preclinical research workflow.

MATERIALS AND METHODS

Synthesis of AuNAs. *Synthesis of Gold Seeds.* 3 nm-gold ultrasmall nanoparticles (USMNPs) were prepared by adding 10 μL of poly(sodium 4-styrenesulfonate) (PSS, 70 kDa, 30% in water; Sigma-Aldrich, #527483) and 200 μL of HAuCl$_4$ aqueous solution (29.4 mM; Alfa Aesar, #36400) to 20 mL of Milli-Q water. Under vigorous stirring, 200 μL of NaBH$_4$ aqueous solution (211 mM; Sigma-Aldrich, #452882) was quickly added, and the solution was stirred for other 2 min. After 10 min, the solution became red.

Synthesis of Gold Arrays. The arrays were formed by slowly adding 75 μL of poly(L-lysine) (PL, 15−30 kDa, 40 mg/mL in Milli-Q water; Sigma-Aldrich, #7890) to the reaction mixture. After 20 min of stirring at room temperature, the arrays were collected by 3 min of centrifugation at 17 092 rcf and resuspended in 2 mL of Milli-Q water.

Synthesis of Gold Nanoarchitectures (AuNAs). The silica shell was formed according to the following modified Stöber protocol. After being shortly sonicated, the array suspension was added to 70 mL of absolute ethanol (Sigma-Aldrich, #24105) previously mixed with 40 μL of tetraethyl orthosilicate (TEOS, 98%; Sigma-Aldrich, #131903) and 2.4 mL of ammonium hydroxide (Sigma-Aldrich, #221228). The mixture was mildly shaken for 3 h at room temperature. The so-formed NAs were collected by 30 min of centrifugation at 3220 rcf. After resuspension in 2 mL of ethanol, NAs were washed once with ethanol and once with Milli-Q water to discard unreacted reagents. Bigger NAs were removed through a short spin (14 s at 14 462 rcf), and the collected supernatant was washed in ethanol and stored in 1 mL of ethanol at −20 °C.

Synthesis of CuNAs. *Synthesis of Copper Seeds.* <2 nm-copper USMNPs were prepared by adding 200 μL of 100 mM reduced L-glutathione solution (Sigma-Aldrich, #G4251) and 200 μL of CuSO$_4$ aqueous solution (25 mM; Sigma-Aldrich, #209198) to 20 mL of Milli-Q water. After the solution had become milky, 200 μL of NaBH$_4$ aqueous solution (211 mM) was quickly added. The mixture was stirred for 2 min; then, 10 μL of PSS (70 kDa, 30% in water) was added, and the reaction stirred for 10 min becoming ocher.

Synthesis of Copper Arrays. 75 μL of PL (15−30 kDa, 40 mg/mL in Milli-Q water) was slowly added to form the arrays, and the mixture was stirred for 20 min at room temperature. Arrays were collected by 3 min of centrifugation at 17 092 rcf and resuspended in 4 mL of Milli-Q water.

Synthesis of CuNAs. The silica shell was formed via a modified Stöber reaction. 70 mL of ethanol was added to 42 μL of TEOS (98%) and gently shaken for 5 min. Two mL of CuNPs arrays was added, followed by 141 μL of dimethylamine (DMA, 40% stock, 428 mg/mL; Alfa Aesar, #31458). The mixture was stirred for 3.5 h at room temperature. CuNAs were collected by 30 min of centrifugation at 3220 rcf and washed twice with ethanol to remove unreacted precursors. Bigger CuNAs were eliminated through a short spin (14 s at 14 462 rcf), and the recovered supernatant was washed once more in ethanol and stored in 1 mL of ethanol at −20 °C.

Synthesis of Metal-Free NAs (MFNAs). *Synthesis of Polymeric Arrays.* 10 μL of PSS was added to 20 mL of Milli-Q water. Under sonication, 75 μL of PL was slowly added to the reaction mixture. After 20 min of stirring at room temperature, the arrays were collected by 3 min of centrifugation at 17 092 rcf and resuspended in 2 mL of Milli-Q water.

Synthesis of Metal-Free Nanoarchitectures (MFNAs). The silica shell was formed according to the following modified Stöber protocol. After being shortly sonicated, the array suspension was added to 70 mL of absolute ethanol previously mixed with 40 μL of TEOS and 2.4 mL of ammonium hydroxide. The mixture was mildly shaken for 3 h at room temperature. MFNAs were collected by 30 min of centrifugation at 3220 rcf. After resuspension in 2 mL of ethanol, NAs were washed once with ethanol and once with Milli-Q water to discard unreacted reagents. Bigger NAs were removed through a short

spin (14 s at 14 462 rcf), and the collected supernatant was washed in ethanol and stored in 1 mL of ethanol at −20 °C.

Characterization of NAs. *Dynamic Light Scattering (DLS) and Zeta-Potential Measurements.* DLS was used to measure the hydrodynamic diameter of NAs in a PBS suspension at 25 °C in a 1 mL quartz cuvette on a Zetasizer nano-ZS90 (Malvern Instruments, Malvern, United Kingdom). The NA suspension in ethanol was spun at 14 462 rcf for 2.5 min; ethanol was discarded, and NAs were resuspended in PBS. The nanomaterials were analyzed with a single scattering angle of 90°. Zeta-potential measurements were performed in DTS 1070 standard capillary cells. Hydrodynamic diameter (as zeta average) and zeta-potential were reported as the average of three consecutive measurements.

Electron Microscopy. Transmission electron microscopy (TEM) images were collected using ZEISS Libra 120 (Oberkochen, Germany), operated at 120 kV accelerating voltage. The NA suspension in ethanol was dropped on 300-mesh carbon-coated copper grids and evaporated before image acquisition. TEM images were analyzed using ImageJ software. Particle diameters and silica shell size were measured on at least 100 nanoparticles.

Inductively Coupled Plasma−Mass Spectrometry (ICP−MS) Analysis. Gold and copper amounts in NAs were quantified using an ICP−MS Agilent 7700 (Agilent Technologies, Santa Clara, CA, USA). Samples were predigested in aqua regia made of 3:1 hydrochloric acid (34−37% in HCl, TraceMetal grade; Thermo Fisher Scientific, #A508-P500) and nitric acid (65% Suprapur; Sigma-Aldrich, #1.00441) and then stirred at 200 °C under a microwave irradiation protocol with a CEM Discover SP-D digestion microwave (CEM, Matthews, NC, USA). The solution was diluted with 3 mL of 3% nitric acid solution, and the Au and Cu contents were quantified by analysis against standard calibration curves (gold standard 1000 ppm, Absolute Standards, inc., #56079; copper standard 1000 ppm, Merck KGaA, #1.70314.0100), using 10 ppm of Hg (Mercury standard for ICP TraceCERT, 10 000 ppm; Sigma-Aldrich, #75111) in 3% nitric acid solution as internal standard.

2D Cell Culture. Human pancreatic cancer cell line BxPC-3 (ATCC, #CRL-1687TM) was purchased from American Type Culture Collection (ATCC). BxPC-3 cells were cultured in RPMI 1640 medium (Gibco, #11875093) supplemented with 10% Fetal Bovine Serum (FBS; Gibco, #10500-064), 1 mM sodium pyruvate (Gibco, #11360070), and 1× penicillin−streptomycin (equivalent to 50 U/mL; Gibco, #15140-122). Cells were maintained at 37 °C and 5% CO$_2$.

Cell Viability Assay. The toxicity of AuNAs and CuNAs on BxPC-3 cells was evaluated using a tetrazolium salt, 2-(2-methoxy-4-nitrophenyl)-3-(4-nitrophenyl)-5-(2,4-disulfophenyl)-2*H* tetrazolium, and monosodium salt (WST-8) assay (Tebu-Bio, #KA1385). 10^4 cells/well of BxPC-3 cells were seeded in a 96-well plate and incubated overnight at 37 °C and 5% CO$_2$. The following day, the medium was removed; cells were washed twice with PBS, and viability at time zero (before treatment) was detected. After that, the treatments were added in a final volume of 100 μL/well: untreated cells (complete medium), AuNAs (1, 5, 10 μg/mL Au in complete medium), and CuNAs (0.1, 0.5, 1, and 2 μg/mL Cu in complete medium). BxPC-3 viability was evaluated also upon the 24 h application of MFNAs. The MFNA tested concentrations were calculated considering the amount of silica administered with AuNAs and CuNAs and their metal loading (22.2, 111, and 222 μg/mL NAs). After 24 h of incubation, the treatments were discarded, and cells were washed twice with PBS and incubated overnight at 37 °C and 5% CO$_2$. The viability was monitored until 72 h post-treatment application, and for each experimental time point, cells were incubated with 10% WST-8 reagent solution in complete medium for 2 h. Absorbance at 450 nm was measured by using a microplate reader (Glomax Discovery, Promega, Madison, WI, USA). The percentage of viable cells was calculated by comparing treated cells with untreated cells for each experimental time point (100% viability). Statistical analysis was performed with GraphPad prism 7.0 software.

Metal Content in Cells. The metal content in cells after AuNAs and CuNAs application was assessed using ICP-MS. BxPC-3 cells

were seeded at a density of 4.5×10^5 cells/well in a 6-well plate and incubated overnight at 37 °C and 5% CO_2. The day after, the medium was removed, and cells were washed twice with PBS and incubated with complete medium (control), AuNAs (10 μg/mL Au in complete medium), or CuNAs (1 μg/mL Cu in complete medium) (1 mL/well). After 24 h of incubation, the treatments were discarded; cells were washed twice with PBS, and fresh complete medium was added. At the end point of the experiment (24, 48, or 72 h), cells were detached using Trypsin-EDTA (0.05%) and phenol red (Gibco, #25300054) to collect the pellets. Pellets were dried at 80 °C until constant weight was reached and then transferred into glass pressure vessels. Samples were digested using aqua regia at 100 °C and dried. The residuals were diluted with 2.5 mL of 3% nitric acid solution, and the Au and Cu contents were quantified by analysis against standard calibration curves using 10 ppm of Hg in 3% nitric acid solution as internal standard.

Chorioallantoic Membrane Assay (CAM) Tumor Model. CAM models of pancreatic ductal adenocarcinoma (PDAC) have been produced according to our standardized protocol.[34] Fertilized red Leghorn eggs were purchased from a local supplier and immediately stored at 4 °C upon delivery. At Embryonic Day of Development (EDD) 0, the eggs were cleaned with deionized water and placed in trays in a fan-assisted incubator (FIEM MG 140/200) at 37.5 °C and 47% humidity. Eggs were punctured at EDD 3. PDAC cells (3×10^6 BxPC-3 cells) were grafted on the CAM at EDD 6. Prior to the grafting, BxPC-3 cells were resuspended in 30 μL of a 1:1 mixture serum-free medium:Matrigel (CORNING, #354234). Eggs were incubated for 4 days, and on EDD 10, eggs were randomized into three groups per each time point (24, 48, 72 h): control (30 μL serum-free medium), AuNAs (24 μg Au per egg), and CuNAs (2.4 μg Cu per egg). The amount of MFNAs applied as control was calculated by deriving the μg of silica administered while providing 24 μg of Au (500 μg NAs per egg). Prior to application, NAs were resuspended in 30 μL of a serum-free medium. The tumor dimensions were measured by using a portable digital microscope (DinoCapture 2.0) before the treatment application (EDD 10) and during the entire experimental window (from EDD 11 to EDD 13). Tumor volumes were derived using the formula 1/2(length $\times$ width^2), where the length and width are the longest and shortest measurements, respectively. Tumors and lower CAM were harvested on EDD 11, 12, and 13 depending on the treatment group. Samples were stored at −80 °C or immediately processed for further biological assays. Statistical analysis was performed with GraphPad prism 7.0 software.

RNA Extraction and Real Time PCR (qRT-PCR). Cell pellets were collected to further investigate the expression of EMT-related genes by using real time PCR (qRT-PCR). BxPC-3 cells were seeded at a density of 2.55×10^5 cells/well in a 6-well plate and incubated overnight at 37 °C and 5% CO_2. The day after, the medium was removed, and cells were washed twice with PBS and incubated with complete medium (control), AuNAs (5 or 10 μg/mL Au in complete medium), or CuNAs (0.5 or 1 μg/mL Cu in complete medium) (1 mL/well). After 24 h of incubation, the treatments were discarded; cells were washed twice with PBS, and fresh complete medium was added. At the final end point of the experiment (24, 48, or 72 h), cells were detached using Trypsin-EDTA (0.05%) to collect the pellets. Pellets were stored at −20 °C and then used to extract RNA.

The cell pellets and the harvested tumors from CAM were mechanically minced into pieces by using a plastic pestle. RNA was extracted using a Nucleospin RNA plus kit (MACHEREY-NAGEL, #740984.50) following the manufacturer's instructions. The extracted RNA samples were quantified using a UV5Nano (Mettler-Toledo, Columbus, OH, USA) and immediately processed or stored at −80 °C. Agarose gel electrophoresis was employed to evaluate the extraction efficiency and the quality of RNA. RNA (500 ng) was reverse transcribed for cDNA synthesis using an iScript cDNA Synthesis Kit (Biorad, #1708891). cDNA (500 ng) was diluted 1:10 in nuclease-free water before use. Quantitative real-time polymerase chain reaction (qRT-PCR) was performed with iTaq Universal SYBR Green Supermix (Biorad, #1725121) for cell pellet-derived samples, whereas for CAM-derived samples, Ssdo Advanced SYBR Green

(Biorad, #1725271) was used. qRT-PCR samples were prepared with 2.5 ng of cDNA template (1 μL of 50 ng of cDNA) in a final volume of 10 μL. Glyceraldehyde 3-phosphate dehydrogenase (GAPDH) was used as a housekeeping gene and as a loading control. The sequences of the primers used are listed in Table 1. All samples were analyzed in

Table 1. Primer Sequences for qRT-PCR

primer	sequence (5′ → 3′)
GAPDH forward	AGAAGGCTGGGGCTCATTT
GAPDH reverse	AGTCTTCTGGGTGGCAGTGAT
E-cadherin forward	ACAGGAACACAGGAGTCATC
E-cadherin reverse	TGTTGCTGTTGTGCTTAACC
Snail forward	TCCAGAGTTTACCTTCCAGC
Snail reverse	AGAGTCCCAGATGAGCATTG
Vimentin forward	GATGTTGACAATGCGTCTCTG
Vimentin reverse	TGTTCCTGAATCTGAGCCTG
Twist forward	CTTCCTCTACCAGGTCCTC
Twist reverse	CAGACCGAGAAGGCGTAG
MMP9 forward	AGACCTGGGCAGATTCCAAAC
MMP9 reverse	CGGCAAGTCTTCCGAGTAGT

duplicate. The amplification curves were visualized using a SYBR Green Analysis on Applied Biosystems Instrument (7300) (Thermo-Fisher Scientific, Waltham, MA, USA). The thermal cycling program for amplification was: 95 °C for 10 min and 40 cycles at 95 °C for 15 s, 58 °C for 30 s, and 72 °C for 30 s. Relative gene expression levels were calculated using the $2^{-\Delta\Delta Ct}$ method.[37] Statistical analysis was performed with GraphPad prism 7.0 software.

Western Blot. The harvested tumors from CAM were minced in RIPA buffer solution (Pierce, #89901) supplemented with Pierce protease inhibitor (Thermo-Fisher, #A32963), and incubated in ice for 30 min. After 30 min of centrifugation at 18 630 rcf at 4 °C, the supernatants were collected. A standard calibration curve of bovine serum albumin (BSA) solutions was generated using a Pierce BCA protein assay kit (#23225). The protein concentrations were then determined reading the absorbance at 562 nm. 30 μg of proteins was mixed with gel loading buffer, loaded in a polyacrylamide gel for SDS-PAGE (Invitrogen, #XP04200BOX), and transferred to a nitro-cellulose membrane (Biorad, #1704271). The membrane was then incubated with a proper blocking solution of 5% powdered milk (Biorad, #170-6404) or 5% BSA (Sigma-Aldrich, #A1470) dissolved in 1× TRIS-buffered saline with 0.1% Tween-20 solution (TBST) (Sigma-Aldrich, #P9416) for 1 h at room temperature. The membranes were then incubated overnight at 4 °C with the respective monoclonal antibodies: α-tubulin (Sigma-Aldrich, no. T6074), E-cadherin (Cell Signaling Technology, no. 24E10), Snail (Santa Cruz Biotechnology, no. sc271977), and Vimentin (Cell Signaling Technology, #D21H3). The day after, the membranes were washed three times with 1× TBST and incubated with the corresponding HRP-conjugated secondary antibodies (Goat antirabbit: Biorad, #170-6515; Goat antimouse: Biorad, #170-6516) for 1 h at room temperature. Further washings in TBST were performed before the detection of the protein bands through an enhanced chemilumines-cence (ECL) kit (Biorad, no. 170562) and Biorad Chemidoc MP Imaging System (Bio-Rad, Hercules, CA, USA). Densitometry analysis was performed by using ImageJ software. Statistical analysis was performed with GraphPad prism 7.0 software.

DNA Extraction: *Alu* PCR. The harvested lower CAM samples were processed using Nucleospin (MACHEREY-NAGEL, #740100.250) to extract DNA following the manufacturer's instruction. To promote enzymatic lysis, the tissues were mechanically homogenized with a plastic pestle. Samples were then incubated with 10 μL of proteinase K (1−3%) and lysis buffer for 30 min at 56 °C on a thermal shaker at 700 rpm. The lysates were loaded onto a column to isolate the DNA, which was then eluted with 200 μL of the elution buffer. UV5Nano (Mettler-Toledo) was used to quantify the extracted DNA, whose integrity was further evaluated by agarose gel
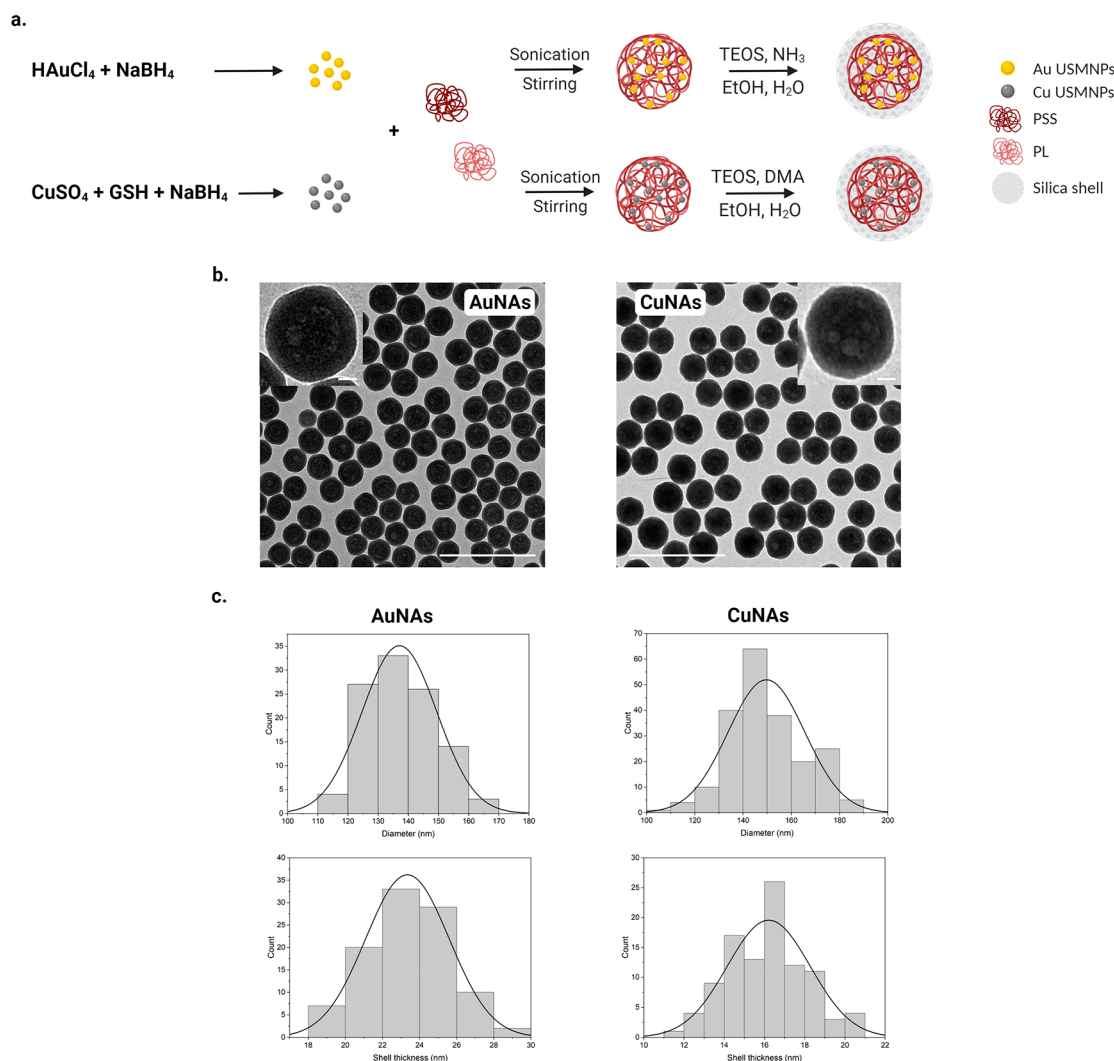
Figure 1. Synthesis and characterization of NAs. (a) Scheme of NAs synthesis. Gold or copper ultrasmall metal nanoparticles (USMNPs) are embedded in a polymeric core shielded by a silica shell produced according to a modified Stöber reaction. DMA, dimethylamine; EtOH, ethanol; TEOS, tetraethyl orthosilicate; PL, poly(L-lysine); PSS, poly(sodium 4-styrenesulfonate). (b) Wide-area TEM image of NAs. Scale bar: 500 nm. The inset is a zoomed-in view of a single nanoarchitecture. Scale bar: 20 nm. (c) Size distribution of NAs diameter (top) and silica shell thickness (bottom) calculated using ImageJ on at least 100 NAs visualized with TEM.

electrophoresis. The DNA samples were either immediately processed or stored at 4 °C. To detect human cancer cells in chick tissues, 30 ng of total DNA was used for the amplification of *Alu* sequences with forward primer: 5′-CAGGCGGATCATGAGGTCAG-3′; reverse primer: 5′-CAGTGGCGTGATCTCAGCTC-3′. qRT-PCR was performed using the Ssdo Advanced SYBR Green (Biorad, no. 1725271) with a final sample volume of 10 μL. The thermal cycling program for amplification of *Alu* sequences was: 98 °C for 5 min followed by 40 cycles of 98 °C for 15 s, 60 °C for 30 s, and 72 °C for 30 s. SYBR Green Analysis on an Applied Biosystems Instrument (7300) was used to visualize the amplification curves. The approximate number of human cancer cells in the lower CAM was calculated from a calibration curve obtained by increasing the number (10 to 100000) of BxPC-3 cells added to the lower CAM of non-grafted eggs. The calibration curve was obtained by plotting the *Alu* threshold cycle as a function of $\log_{10}$ of the number of BxPC-3 cells.[34] Statistical analysis was performed with GraphPad prism 7.0 software.

■ RESULTS AND DISCUSSION

NAs are biodegradable ultrasmall-in-nano architectures in which ultrasmall metal nanoparticles (USMNPs) of gold (3 nm) or copper (<2 nm) are embedded in a polymeric matrix (Figure 1a). The polymeric matrix is formed by polymers of opposite charge, namely, poly(sodium 4-styrenesulfonate) (PPS, negatively charged) and poly(L-lysine) (PL, positively charged). The polymeric templates enclosing USMNPs are embedded in a silica capsule formed via a modified Stöber reaction (final diameter: ~150 nm).[14,33] The silica shell protects the inner core and provides a modifiable surface for active targeting purposes.[38] The synthetic protocol is standardized with a high batch-by-batch homogeneity, and its versatility is demonstrated by the possibility to include various metals (gold, silver, platinum, copper) and/or active molecules or dyes.[39,40] As we have already demonstrated, plasmon USMNPs enclosed in NAs are efficiently excreted after intravenous injection or intranasal instillation in healthy mice.[15−17] The hydrodynamic diameter and zeta potential of NAs were measured using Dynamic Light Scattering (DLS), whereas the size was assessed through Transmission Electron Microscopy (TEM) imaging (Figure 1b,c), and the metal content was determined using Inductively Coupled Plasma−Mass Spectrometry (ICP−MS) (Table 2). The similar morphological features of AuNAs and CuNAs allow to

correlate the biological effects to the chemical nature of the inner metal.[33]

Table 2. Comparison of the Principal Features of AuNAs and CuNAs

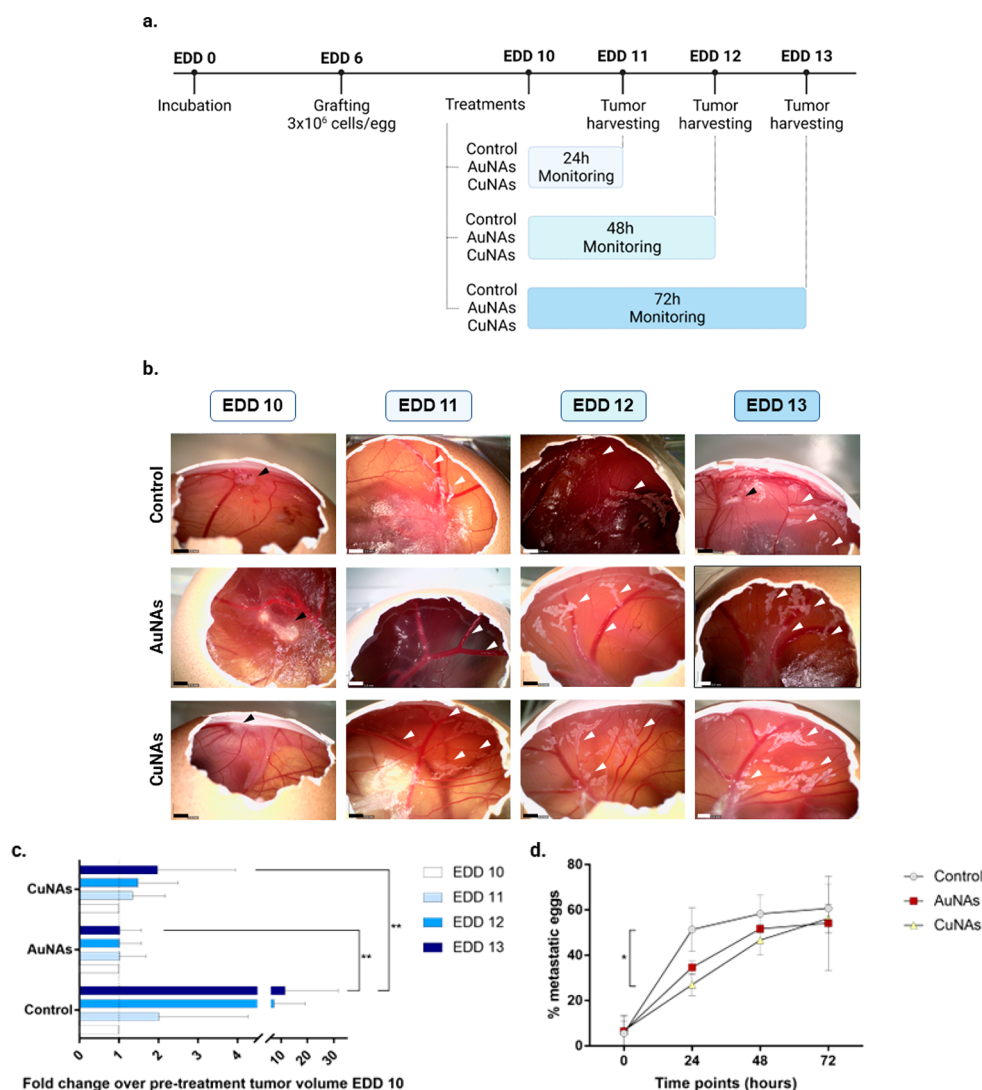|	AuNAs	CuNAs
Average diameter (TEM, nm)	137 ± 12	150 ± 16
Shell thickness (TEM, nm)	23.3 ± 2.2	16.2 ± 2.1
Hydrodynamic diameter in PBS (DLS, nm)	203.1 ± 1.9	403 ± 10
Zeta potential in PBS (mV)	−20.6 ± 0.4	−15.2 ± 0.7
Metal loading (% w/w)	4.5	1.1

The *in vitro* studies were performed on the BxPC-3 human pancreatic cancer cell line. The BxPC-3 cell line is among the most invasive PDAC cell line, bearing mutations on TP53, SMAD4, and CDKN2A, whereas KRAS is in its wild-type sequence.[41] Despite the crucial role of KRAS mutation in PDAC, its wild-type sequence does not compromise the metastatic behavior of BxPC-3 cells, as there is not a specific mutation for metastasis development.[42] Moreover, the metastatic potential of BxPC-3 can be explained through the overexpression of EIF5A protein, which is considered decisive in the evolution of PDAC metastasis.[43,44] As a consequence, BxPC-3 cell-derived tumors develop liver and lymph node metastasis in transplantation models, providing a good model for PDAC metastasis studies.[45] Metal-free NAs (MFNAs) (Figure 1SI) have been employed as a control to assess the effect of the nanoarchitectures without metals on the viability of cells. Then, the cytotoxicity of AuNAs and CuNAs on BxPC-3 was evaluated at the same silica concentrations. NAs were incubated for 24 h, and the viability of the NAs-treated cells was compared to the untreated (complete medium) samples (Figure 2a,b). As expected, AuNAs showed no toxicity at all the tested concentrations, while the CuNAs concentration above 1 µg/mL Cu resulted slightly toxic. The AuNAs transiently prompted cell metabolism until degradation of the silica shell. The different behavior of AuNAs compared to other AuNPs is associated with the different morphology of the nanoplatforms.[46] For concentrations ≤1 µg/mL Cu, CuNAs stimulated cell metabolism at 24 h post-incubation and repressed it at 48 h. Interestingly, cell metabolism, hence cell
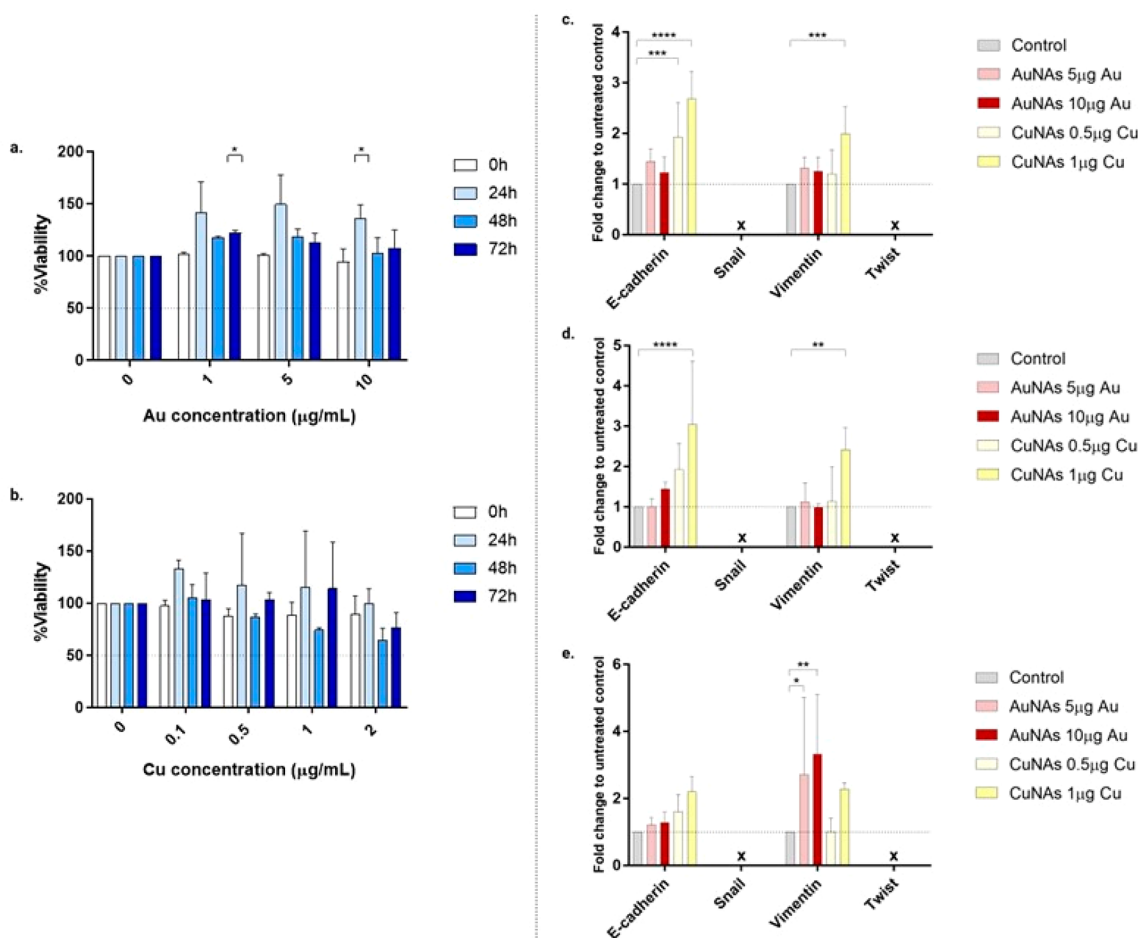
Figure 2. Viability and EMT-related gene expression in BxPC-3 cells after NAs treatment. Left panel: Viability assays on BxPC-3 cells after a 24 h incubation with (a) AuNAs or (b) CuNAs. % Viability was compared to the control represented by untreated cells (complete medium) for each time point. Data are reported as mean ± standard deviation from two independent experiments performed in triplicate. Statistical analysis was performed using the multiple *t* test with Holm-Sidak's multiple comparison test, *p < 0.05, **p < 0.01, ***p < 0.001, ****p < 0.0001. Right panel: qRT-PCR on BxPC-3 cells after AuNAs or CuNAs application at different concentrations. The cells were incubated with the treatment for 24 h, and cell pellets were collected after (c) 24 h, (d) 48 h, and (e) 72 h. Gene expression was normalized over the control (untreated cells). Data are reported as mean ± standard deviation from three independent experiments, each performed in duplicate. Statistical analysis was performed using two-way ANOVA with Dunnett's multiple comparison test, *p < 0.05, **p < 0.01, ***p < 0.001, ****p < 0.0001.

Figure 3. (a) Scheme of the experimental protocol. On EDD 6, BxPC-3 cells were grafted on CAM. After 4 days, tumor-bearing eggs were randomized into three groups (Control, AuNAs, CuNAs) per each time point. Tumors and metastasis were monitored until the end point at which the tumors were harvested (24, 48, or 72 h). (b) Representative images of tumors and metastasis (black and white arrows, respectively) of the same egg from EDD 10 to EDD 13 for the different treatments. Scale bar: 2 mm. Metastasis grew over time, with changes in tumor size and morphology for all of the treatments. (c) Tumor volume fold change compared to EDD 10. AuNAs and CuNAs significantly reduced the tumor growth compared to the untreated (control) eggs. Data are reported as mean ± standard deviation (control: $n = 10$, AuNAs: $n = 11$, CuNAs: $n = 10$). Statistical analysis was performed through two-way ANOVA, with Dunnett's comparison, *$p < 0.05$, **$p < 0.01$, ***$p < 0.001$, ****$p < 0.0001$. (d) Metastasis in the upper CAM displayed as a percentage of metastatic upper CAM over the number of eggs. AuNAs and CuNAs slowed cancer cell migration in the upper CAM. Data are reported as mean ± standard deviation from two independent experiments with n_1 and n_2 number of eggs each (0 h: control $n_1 = 12$ $n_2 = 18$, AuNAs $n_1 = 8$ $n_2 = 22$, CuNAs $n_1 = 9$ $n_2 = 22$; 24 h: control $n_1 = 12$ $n_2 = 18$, AuNAs $n_1 = 8$ $n_2 = 22$, CuNAs $n_1 = 9$ $n_2 = 22$; 48 h: control $n_1 = 8$ $n_2 = 12$, AuNAs $n_1 = 8$ $n_2 = 15$, CuNAs $n_1 = 5$ $n_2 = 15$; 72 h: control $n_1 = 4$ $n_2 = 7$, AuNAs $n_1 = 3$ $n_2 = 8$, CuNAs $n_1 = 3$ $n_2 = 7$). Statistical analysis was performed through two-way ANOVA, with Sidak's comparison, *$p < 0.05$, **$p < 0.01$, ***$p < 0.001$, ****$p < 0.0001$.

viability, increased again close to the levels of untreated samples after 72 h. This trend can be related to copper release in cells. At 24 h post-incubation, the small leakage of copper from the whole NAs stimulated cell viability.[33] After the biodegradation of the silica shell, the burst release of copper overcame the buffering capacity of cells.[47] With non-excessive damage, the efflux systems may have promoted the excretion of the exceeding ions to restore the homeostatic intracellular copper concentration. Otherwise, massive copper-induced damage can be unrecoverable (>1 μg/mL Cu). Overall, CuNAs affect the viability of BxPC-3 cells more than AuNAs, likely due to the different chemistry of the metals. Indeed,

differently from gold, copper USMNPs can be oxidized, releasing ions that can covalently interact with proteins.[25] These findings provided suitable concentrations of NAs to evaluate their antimetastatic activity without harming cells. As cytotoxic NAs levels should be avoided, Au concentrations of 5 and 10 μg/mL and Cu concentrations of 0.5 and 1 μg/mL (molar ratio Cu:Au 1:3) were selected for the following *in vitro* assays.

The antimetastatic efficiency of AuNAs and CuNAs was first evaluated *in vitro* through the alteration of the EMT-related genes expression over time (Figure 2c,d,e). In cancer cells undergoing metastasis, EMT promotes the downregulation of
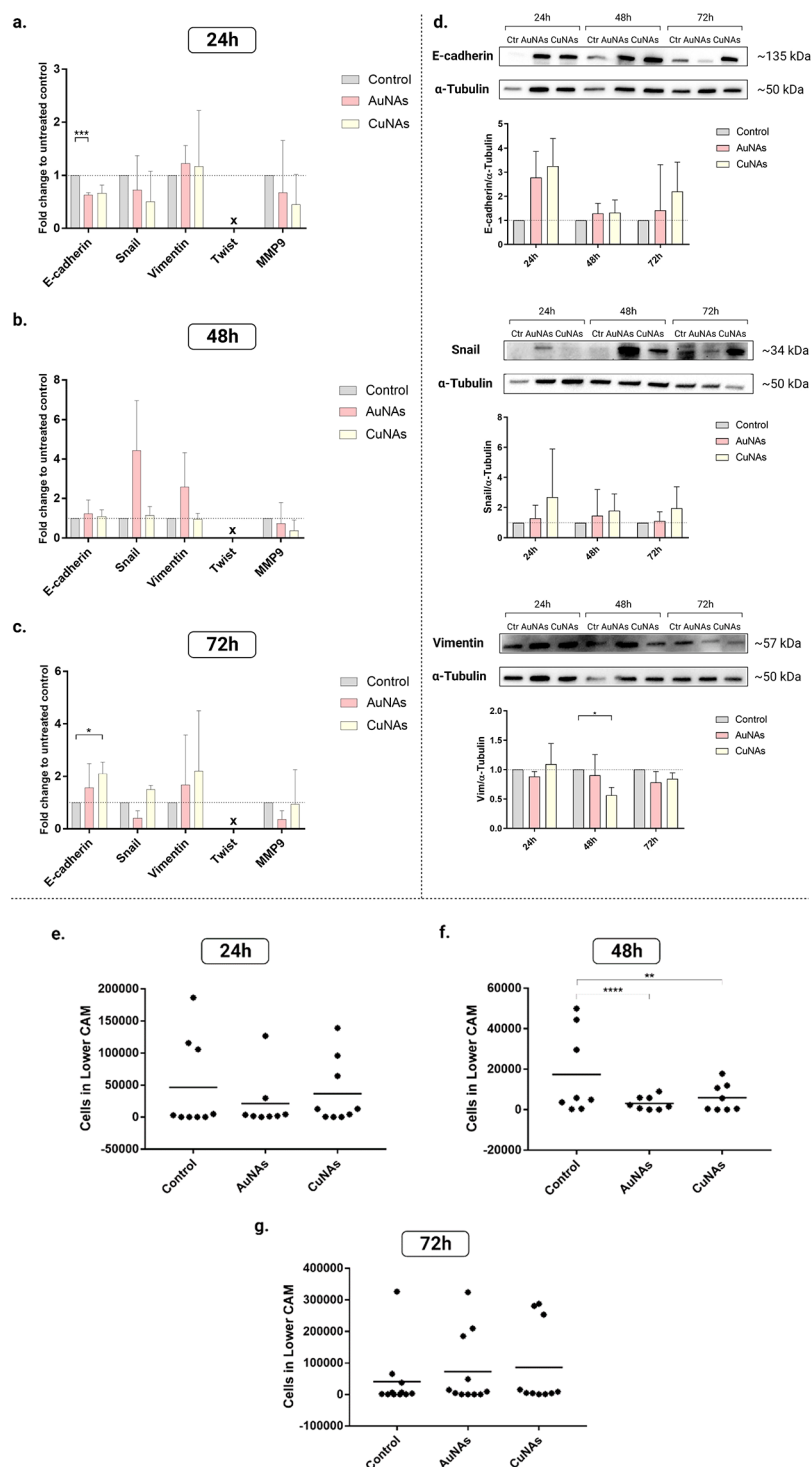
Figure 4. Evaluation of NAs effects on the regulation of EMT-related genes and proteins on CAM tumors and on tumor cell migration to the lower CAM. Top panel: qRT-PCR analysis on tumors harvested at 24 h (a), 48 h (b), and 72 h (c) from the CAM treated with AuNAs or CuNAs. Data are reported as mean ± standard deviation ($N = 3$). Statistical analysis was performed through the multiple t test, Holm-Sidak's method, *$p < 0.05$, **$p < 0.01$, ***$p < 0.001$, ****$p < 0.0001$. (d) Protein expression in CAM tumors. Western Blot analysis on the production of EMT-associated proteins on tumors harvested at 24, 48, and 72 h from CAMs treated with AuNAs or CuNAs. The expression of the proteins was quantified by normalizing over the intensity of the band of α-tubulin. Densitometry analysis was performed using ImageJ software. The antimetastatic properties of NAs observed in the upper CAM were confirmed by the regulation of EMT-related genes and proteins. Data are reported as mean ± standard deviation ($N = 3$). Statistical analysis was performed through the multiple t test, Holm-Sidak's method, *$p < 0.05$, **$p < 0.01$, ***$p < 0.001$, ****$p < 0.0001$. Quantification of the cancer cells in the lower CAM by qRT-PCR analysis of *Alu* expression at 24 h (e), 48 h (f), and 72 h (g). 24 h: control $n = 9$, AuNAs $n = 8$, CuNAs $n = 9$; 48 h: control $n = 8$, AuNAs $n = 8$, CuNAs $n = 8$; 72 h: control $n = 11$, AuNAs $n = 11$, CuNAs $n = 10$. Corroborating the delay in metastasis spreading in the upper CAM at 24 h; NAs significantly reduce the number of cancer cells in the lower CAM at 48 h. Statistical analysis was performed through the multiple t test, Welch's test, *$p < 0.05$, **$p < 0.01$, ***$p < 0.001$, ****$p < 0.0001$.

endothelial genes (e.g., CDH1 coding for E-cadherin) and the upregulation of mesenchymal genes (e.g., SNAI1 coding for Snail, VIM coding for Vimentin, and TWIST1).[3] As a consequence, an antimetastatic agent should revert this process to avoid cell migration. After a 24 h incubation with NAs, cell pellets were collected at 24, 48, and 72 h and the expression of EMT-related genes was quantified and normalized over the untreated groups (control). Real time PCR (qRT-PCR) was employed for this purpose. One day after NAs application, the expression of the E-cadherin encoding gene was significantly increased by CuNAs but not by AuNAs. This effect lasted for 48 h, probably due to the cell excretion and restoring mechanisms. Among the investigated mesenchymal genes, only Vimentin was expressed in the 2D cultures of BxPC-3. In accordance with literature, Snail and Twist genes were not detected by qRT-PCR after 40 cycles in BxPC-3 2D cell cultures.[48] This is due to the role of Snail in regulating the cell−extracellular matrix interactions, which is not stimulated in *in vitro* models owing to the absence of the extracellular matrix.[49] The cooperativity of the transcription factors Snail and Twist may result in a lack of expression of both.[50] In conclusion, despite being more toxic than AuNAs in 2D experiments, CuNAs better regulated the expression of the E-cadherin encoding gene in 2D cell cultures. The correlation between USMNPs in the cells and the regulation of EMT-related genes was confirmed assessing the metal uptake after a 24 h incubation with AuNAs and CuNAs. The efficiency in metal uptake by BxPC-3 cells was evaluated by collecting treated cell pellets at 24, 48, and 72 h to quantify the metal content by using ICP-MS (Figure 2SI). In AuNAs-treated samples, the internalized Au was 8% of the administered dose at 24 h and 4.5% after 72 h. CuNAs application significantly boosted the copper content compared with the untreated cells. After 48 h, copper levels increased by 50% compared to 24 h, which is consistent with the nanoarchitecture design and degradation timing. It is interesting to notice that AuNAs administration did not affect the endogenous copper levels. Noteworthy, the transient accumulation of both metals supports the transient effects of NAs. These results suggest that the nature of the USMNPs influences the regulation of gene expression. In particular, the main effects in the regulation of the EMT-related genes have been recognized after silica shell biodegradation, which caused the massive release of USMNPs. Nevertheless, the *in vitro* model showed several limits for the evaluation of the antimetastatic effect of NAs. Indeed, the mesenchymal genes involved in cell−matrix interactions were not expressed by the 2D cultured cells. For this reason, we established an alternative *in vivo* model able to mimic the heterogeneity of the metastatic phenomenon: the chorioallantoic membrane (CAM) model.[35] Indeed, the rapid tumor development and the easy monitoring of primary tumor and metastasis allow for multiple time point studies in compliance with 3R principles, presenting CAMs as a suitable model for metastasis evaluation. As in the murine model, the dynamic tumor microenvironment in the CAM provides several obstacles for cancer cells to infiltrate blood or lymphatic vessels and subsequently extravasate in different parts of the CAM or of the chicken embryo.[35] If disseminated cancer cells survive, then metastasis can develop. For this reason, the CAM model has been employed to study the metastatic phenomenon of some cancers.[51,52] However, previous works either focused on different markers of cell invasion or did not apply a constant monitoring of the

metastasis development.[52−54] On the contrary, we evaluated and compared the EMT phenomenon and metastasis progression in the upper and lower CAM (respectively, the area near the opened window on the egg and the opposite one). To the best of our knowledge, the evolution of BxPC-3 metastasis and the related EMT-gene expression over time has not been previously evaluated in CAM models, and, for this reason, we examined and correlated the evolution of metastasis on the upper and lower CAM at 24, 48, and 72 h after treatment.[34] On Embryonic Day of Development (EDD) 6, 3.0×10^6 BxPC-3 cells/egg were grafted to generate tumor masses on the membrane of the chicken embryo with a grafting rate of approximately 57%. On EDD 10, the tumor-bearing eggs were randomized into three groups (control, AuNAs 24 μg Au, CuNAs 2.4 μg Cu) per each time point (24 h − EDD 11, 48 h − EDD 12, 72 h − EDD 13) (Figure 3a). Grafted PDAC cells develop plaque tumors below the CAM surface that are avascular until the pre-existing CAM vasculature penetrates the tumor tissue.[36] The amount of gold applied to the tumor was comparable to our previous works, while copper concentration was 10-fold lower than gold.[18] The difference in the metal content reflected the results of the *in vitro* studies. The activity of NAs was evaluated using control eggs as reference in the respective experimental group. Tumor volume and metastasis on the upper CAM were monitored until each end point, wherein tumors were also harvested. Embryo viability was not affected by NAs application, confirming the employment of a safe metal concentration, as emerged from the 2D studies. During the experimental window, the morphology and the size of the primary tumors changed together with the appearance of metastasis. Interestingly, metastasis grew along the tumor vessels with an oak leaf-like shape (Figure 3b). On EDD 11 (24 h), metastases in control eggs were significantly more disseminated than in NAs-treated eggs. The application of NAs delayed the incidence of metastasis in the upper CAM over time, eventually with no differences compared to the control (Figure 3d). Both AuNAs and CuNAs controlled the primary tumor growth at the tested concentrations (Figure 3c). Together with a reduction in metastasis incidence during the early time points, NAs inhibited the growth of the primary tumor, reducing cancer cell migration to metastatic niches. The parallel shrinking tumor effect of NAs can help to meet the regulatory requirements for the approval of antimetastatic agents.[3] We confirmed that the USMNPs are the active agents in NAs and were crucial for limiting tumor growth and slowing metastasis spreading by performing comparative assays with MFNAs (NAs without metals). Indeed, the application of MFNAs did not show any effect as the lack of USMNPs resulted in no activity on the tumor volume nor on the metastasis spreading in the upper CAM (Figure 3SI). Therefore, it is reasonable to link the antitumoral and antimetastatic activities of AuNAs and CuNAs to the USMNPs rather than the silica or polymeric components of NAs.

The macroscopic delay in metastasis development observed in the upper CAM after NAs treatment was further confirmed by NAs regulation of the expression of EMT-related genes in harvested tumors (Figure 4a−c). Besides the genes explored in the *in vitro* studies, we evaluated the expression of the MMP9 encoding gene in CAM-derived tumors. MMP9 is a matrix metalloproteinase that cleaves the extracellular matrix to favor cell migration and whose high expression correlates with poor prognosis in cancer patients.[55] An antimetastatic treatment

should downregulate the expression of the MMP9 encoding gene, which was not evaluated in 2D models of BxPC-3 cells as they lack the extracellular matrix. For the same reason, the Snail gene was detected in CAM-derived tumors and not in 2D models. Twist gene was still not detected, probably due to a different timing of expression. The outcome of NAs application on the EMT phenomenon was evaluated through quantification of gene and protein expression. The regulation of the epithelial gene encoding for E-cadherin reflected E-cadherin expression in the harvested CAM tumors at 48 and 72 h (Figure 4d). While E-cadherin encoding gene was downregulated by AuNAs and CuNAs at 24 h, the protein production was stimulated by both NAs with the same intensity, although not significantly. Interestingly, 72 h after AuNAs application, the E-cadherin encoding gene was upregulated while Snail was downregulated. Indeed, Snail may act as a transcriptional repressor of the E-cadherin gene; therefore, an increased expression of the latter might be associated with a downregulation of the first.[56] The modulation of Snail protein production by AuNAs did not reflect the trend of the Snail transcription factor. CuNAs likely stabilized Snail protein at 72 h due to the release of copper before and after NA degradation. Indeed, the increase of copper stimulates the copper-dependent lysyl oxidase-like proteins that can stabilize Snail protein.[57] The expression of the MMP9 encoding gene was downregulated by both AuNAs and CuNAs during the entire experimental window. Even though there was not a regulation on the expression of the Vimentin gene, the protein expression was affected by NAs application. The downregulation of Vimentin protein induced by AuNAs and CuNAs started at 24 and 48 h, respectively. In both cases, this inhibition was maintained until 72 h. Noteworthy, CuNAs significantly downregulated the expression of Vimentin protein at 48 h. Taken together, these findings confirm the interconnection among epithelial and mesenchymal genes involved in EMT and the effect of the fluctuation of intracellular copper levels on protein production. As expected, the maximum effect of both NAs on gene expression and protein production was recognized 48 h after the application. This observation highlights that the metabolization of NAs components leads to a transient effect at these concentrations. It is interesting to note that, while on 2D cultured cells CuNAs performed better than AuNAs in slowing down cell migration, the effect of CuNAs in CAM models was less impactful than AuNAs on gene and protein expression of EMT-related factors. As AuNAs exerted better effects on the mesenchymal factors than CuNAs, they may contrast cancer cell migratory properties more efficiently. Such contraposition stresses the fundamental role of alternative *in vivo* models in evaluating the efficacy of anticancer treatments. These conclusions were further supported by the absence of EMT-gene regulation in MFNA-treated CAM tumors at 48 h (Figure 3SI), which suggests the link between USMNPs comprised in NAs and the therapeutic action.

NAs impact on the expression of EMT-related genes and proteins eventually influenced the ability of pancreatic cancer cells to spontaneously migrate toward the distal region of the lower CAM (Figure 4e−g). As reported in Sarogni *et al.*, a calibration curve of BxPC-3 cells in lower CAM from non-grafted embryos has been used to quantify the cells in the lower CAM from treated eggs depending on the detected *Alu* threshold cycle.[34] *Alu* sequences are primate-specific short interspersed elements that are not expressed in avian DNA.[58]

Such short sequences can be used to specifically identify the presence of human cells among chicken tissue, as lower CAM, using qRT-PCR.[59] BxPC-3 cells were detected in the lower CAM in all of the treatment groups at the selected time points. At 24 h, AuNAs and CuNAs did not reduce the number of cells in the lower CAM, in agreement with the modulation of EMT-related genes. On the other hand, the nanoarchitectures significantly reduced the number of cancer cells in the lower CAM at 48 h because of the efficient EMT-gene modulation, especially for AuNAs. MFNAs did not alter the number of cancer cells migrated to the lower CAM after 48 h; hence, the antimigratory tendency can be associated with the presence of USMNPs rather than the other NA components (Figure 3SI). Remarkably, a synchronization between the metastasis percentage in the upper CAM and the number of cancer cells detected in the lower CAM has been observed. Indeed, the lower percentage of the upper CAM bearing metastasis induced by NAs at 24 h was followed by a reduced cell migration to the lower CAM at 48 h. Overall, the time dependence of the NA antimetastatic effect was reflected in the upper CAM as a percentage of metastatic CAMs, in gene expression and protein production in tumor, and finally in the effective number of cancer cells metastasized in the lower CAM. At 72 h, the effect of NAs terminated. This can be correlated to the single application of NAs that can only transiently reduce the migration of pancreatic cancer cells, which are known for their aggressiveness and migratory tendency.[8]

◼ CONCLUSIONS

Overall, our findings suggest that rationally nanostructured gold and copper modulate pancreatic cancer metastasis by acting on both gene expression and cell migratory properties. The different outcome among *in vitro* and *in ovo* models stresses the importance of screening novel potential treatments with complex models able to mimic the metastatic environment. Albeit the effect of NAs did not persist more than 3 days, we may suppose that repeated doses of NAs could result in longer and stronger effects on metastasis. Among the tested metals at non-cytotoxic concentration, AuNAs modulated the metastatic cascade better than copper. To assess whether the copper effect could be mediated by other cellular pathways, the expression of antioxidant genes may be further evaluated as they are involved in the metastatic process. Moreover, further investigations on the antimetastatic effects of multiple or combined treatments, such as with radiotherapy, would be interesting due to the potential radiosensitizing activity of gold USMNPs. Indeed, a combined treatment may promote better outcomes by reducing the risk of resistance development. It should be noted that the non-persistence behaviors of AuNAs can support their clinical translation. Together with these findings, we introduced an alternative biomodel to evaluate PDAC metastasis and the effects of antimetastatic treatments over time. Despite the suitability of CAM in preclinical research, some limitations that constrain their employment should be considered, such as (i) the short experimental window that reduces the follow-up period and (ii) the lack of a human immune system that does not completely allow to replicate the tumor−host immune system interactions. On the other hand, CAMs perfectly fit for preliminary screening of antimetastatic agents in agreement with the 3R concept. In general, gold and copper ultrasmall-in-nano architectures modulate tumor growth and metastasis spreading in *in ovo*

models, and these findings represent a promising step toward the establishment of novel nanostrategies for the control of pancreatic cancer metastasis.

■ ASSOCIATED CONTENT

Ⓢ Supporting Information

The Supporting Information is available free of charge at https://pubs.acs.org/doi/10.1021/acsanm.3c05299.

> Viability of BxPC-3 cells after MFNA treatment; metal uptake in 2D culture of BxPC-3 cells; tumor volume fold change; metastasis in the upper CAM; MFNA effects on the regulation of EMT-related genes on CAM tumors; quantification of the cancer cells in the lower CAM; uncropped blot of the investigated proteins in CAM tumors (PDF)

■ AUTHOR INFORMATION

Corresponding Author

Valerio Voliani − *Center for Nanotechnology Innovation@ NEST, Istituto Italiano di Tecnologia, 56127 Pisa, Italy; Department of Pharmacy, School of Medical and Pharmaceutical Sciences, University of Genoa, 16148 Genoa, Italy;* ⦿ orcid.org/0000-0003-1311-3349; Email: valerio.voliani@unige.it

Authors

Agata Zamborlin − *Center for Nanotechnology Innovation@ NEST, Istituto Italiano di Tecnologia, 56127 Pisa, Italy; NEST-Scuola Normale Superiore, 56127 Pisa, Italy*

Patrizia Sarogni − *Center for Nanotechnology Innovation@ NEST, Istituto Italiano di Tecnologia, 56127 Pisa, Italy*

Valentina Frusca − *Center for Nanotechnology Innovation@ NEST, Istituto Italiano di Tecnologia, 56127 Pisa, Italy; Scuola Superiore Sant'Anna, 56127 Pisa, Italy;* ⦿ orcid.org/ 0000-0002-1092-6232

Alessandra Gonnelli − *Center for Nanotechnology Innovation@NEST, Istituto Italiano di Tecnologia, 56127 Pisa, Italy; Radiation Oncology Unit, Pisa University Hospital "Azienda Ospedaliero-Universitaria Pisana", 56126 Pisa, Italy*

Noemi Giannini − *Center for Nanotechnology Innovation@ NEST, Istituto Italiano di Tecnologia, 56127 Pisa, Italy; Radiation Oncology Unit, Pisa University Hospital "Azienda Ospedaliero-Universitaria Pisana", 56126 Pisa, Italy*

Maria Laura Ermini − *Center for Nanotechnology Innovation@NEST, Istituto Italiano di Tecnologia, 56127 Pisa, Italy*

Andrea Marranci − *Fondazione Pisana per la Scienza ONLUS, 56017 S. Giuliano Terme, Pisa, Italy;* ⦿ orcid.org/ 0000-0002-8334-8795

Francesca Pagliari − *Division of BioMedical Physics in Radiation Oncology, German Cancer Research Center, 69120 Heidelberg, Germany*

Chiara Maria Mazzanti − *Fondazione Pisana per la Scienza ONLUS, 56017 S. Giuliano Terme, Pisa, Italy*

Joao Seco − *Division of BioMedical Physics in Radiation Oncology, German Cancer Research Center, 69120 Heidelberg, Germany; Department of Physics and Astronomy, Heidelberg University, 69120 Heidelberg, Germany*

Complete contact information is available at:
https://pubs.acs.org/10.1021/acsanm.3c05299

Author Contributions

A.Z., P.S., V.F., A.G., N.G., M.L.E., A.M., and F.P.: data curation, formal analysis, and investigation. C.M.M. and J.S.: supervision and validation. V.V.: conceptualization, funding acquisition, supervision, and validation. All the authors discussed the data and contributed to writing the manuscript.

Notes

The authors declare no competing financial interest.

■ ACKNOWLEDGMENTS

■ REFERENCES

(1) Siegel, R. L.; Miller, K. D.; Fuchs, H. E.; Jemal, A. Cancer Statistics, 2022. *CA. Cancer J. Clin.* **2022**, *72* (1), 7−33.

(2) Fares, J.; Fares, M. Y.; Khachfe, H. H.; Salhab, H. A.; Fares, Y. Molecular Principles of Metastasis: A Hallmark of Cancer Revisited. *Signal Transduct. Target. Ther.* **2020**, *5*, 28.

(3) Zamborlin, A.; Voliani, V. Gold Nanoparticles as Antiangiogenic and Antimetastatic Agents. *Drug Discovery Today* **2023**, *28* (2), No. 103438.

(4) Zhang, J.; Wang, N.; Li, Q.; Zhou, Y.; Luan, Y. A Two-Pronged Photodynamic Nanodrug to Prevent Metastasis of Basal-like Breast Cancer. *Chem. Commun.* **2021**, *57* (18), 2305−2308.

(5) Dev, A.; Sardoiwala, M. N.; Boddu, M.; Mohanbhai, S. J.; Choudhury, S. R.; Karmakar, S. 4-Oxo-Fenretinide-Loaded Human Serum Albumin Nanoparticles for the Inhibition of Epithelial-Mesenchymal Transition in Neuroblastoma Xenografts. *ACS Appl. Nano Mater.* **2022**, *5* (5), 7540−7548.

(6) Huang, Y.; Hong, W.; Wei, X. The Molecular Mechanisms and Therapeutic Strategies of EMT in Tumor Progression and Metastasis. *J. Hematol. Oncol.* **2022**, *15* (1), 1−27.

(7) Jonckheere, S.; Adams, J.; De Groote, D.; Campbell, K.; Berx, G.; Goossens, S. Epithelial-Mesenchymal Transition (EMT) as a Therapeutic Target. *Cells Tissues Organs* **2022**, *211* (2), 157−182.

(8) Kamisawa, T.; Wood, L. D.; Itoi, T.; Takaori, K. Pancreatic Cancer. *Lancet* **2016**, *388* (10039), 73−85.

(9) Hu, J. X.; Lin, Y. Y.; Zhao, C. F.; Chen, W. B.; Liu, Q. C.; Li, Q. W.; Gao, F. Pancreatic Cancer: A Review of Epidemiology, Trend, and Risk Factors. *World J. Gastroenterol.* **2021**, *27* (27), 4298−4321.

(10) Shi, J.; Kantoff, P. W.; Wooster, R.; Farokhzad, O. C. Cancer Nanomedicine: Progress, Challenges and Opportunities. *Nat. Rev. Cancer* **2017**, *17* (1), 20−37.

(11) Germain, M.; Caputo, F.; Metcalfe, S.; Tosi, G.; Spring, K.; Åslund, A. K. O.; Pottier, A.; Schiffelers, R.; Ceccaldi, A.; Schmid, R. Delivering the Power of Nanomedicine to Patients Today. *J. Controlled Release* **2020**, *326* (April), 164−171.

(12) Sibuyi, N. R. S.; Moabelo, K. L.; Fadaka, A. O.; Meyer, S.; Onani, M. O.; Madiehe, A. M.; Meyer, M. Multifunctional Gold Nanoparticles for Improved Diagnostic and Therapeutic Applications: A Review. *Nanoscale Res. Lett.* **2021**, *16*, 174.

(13) Cassano, D.; Pocoví-Martínez, S.; Voliani, V. Ultrasmall-in-Nano Approach: Enabling the Translation of Metal Nanomaterials to Clinics. *Bioconjugate Chem.* **2018**, *29*, 4−16.

(14) Cassano, D.; David, J.; Luin, S.; Voliani, V. Passion Fruit-like Nanoarchitectures: A General Synthesis Route. *Sci. Rep.* **2017**, *7*, 1−9.

(15) Cassano, D.; Mapanao, A.; Summa, M.; Vlamidis, Y.; Giannone, G.; Santi, M.; Guzzolino, E.; Pitto, L.; Poliseno, L.; Bertorelli, R.; Voliani, V. Biosafety and Biokinetics of Noble Metals: The Impact of Their Chemical Nature. *ACS Appl. Bio Mater.* **2019**, *2* (10), 4464−4470.

(16) Mapanao, A. K.; Giannone, G.; Summa, M.; Ermini, M. L.; Zamborlin, A.; Santi, M.; Cassano, D.; Bertorelli, R.; Voliani, V.

Biokinetics and Clearance of Inhaled Gold Ultrasmall-in-Nano Architectures. *Nanoscale Adv.* **2020**, *2*, 3815−3820.

(17) Zamborlin, A.; Ermini, M. L.; Summa, M.; Giannone, G.; Frusca, V.; Mapanao, A. K.; Debellis, D.; Bertorelli, R.; Voliani, V. The Fate of Intranasally Instilled Silver Nanoarchitectures. *Nano Lett.* **2022**, *22*, 5269−5276.

(18) Sarogni, P.; Mapanao, A. K.; Gonnelli, A.; Ermini, M. L.; Marchetti, S.; Kusmic, C.; Paiar, F.; Voliani, V. Chorioallantoic Membrane Tumor Models Highlight the Effects of Cisplatin Compounds in Oral Carcinoma Treatment. *iScience* **2022**, *25*, No. 103980.

(19) Arvizo, R. R.; Saha, S.; Wang, E.; Robertson, J. D.; Bhattacharya, R.; Mukherjee, P. Inhibition of Tumor Growth and Metastasis by a Self-Therapeutic Nanoparticle. *Proc. Natl. Acad. Sci. U. S. A.* **2013**, *110* (17), 6700−6705.

(20) Ge, E. J.; Bush, A. I.; Casini, A.; Cobine, P. A.; Cross, J. R.; DeNicola, G. M.; Dou, Q. P.; Franz, K. J.; Gohil, V. M.; Gupta, S.; Kaler, S. G.; Lutsenko, S.; Mittal, V.; Petris, M. J.; Polishchuk, R.; Ralle, M.; Schilsky, M. L.; Tonks, N. K.; Vahdat, L. T.; Van Aelst, L.; Xi, D.; Yuan, P.; Brady, D. C.; Chang, C. J. Connecting Copper and Cancer: From Transition Metal Signalling to Metalloplasia. *Nat. Rev. Cancer* **2022**, *22* (2), 102−113.

(21) da Silva, D. A.; Luca, De; Squitti, A.; Rongioletti, R.; Rossi, M.; Machado, L.; Cerchiaro, C. M. L.; Copper, G. in Tumors and the Use of Copper-Based Compounds in Cancer Treatment. *J. Inorg. Biochem.* **2022**, *226*, No. 111634.

(22) Molinaro, C.; Martoriati, A.; Pelinski, L.; Cailliau, K. Copper Complexes as Anticancer Agents Targeting Topoisomerases I and II. *Cancers (Basel).* **2020**, *12* (10), 2863.

(23) Maliki, M.; Ifijen, I. H.; Ikhuoria, E. U.; Jonathan, E. M.; Onaiwu, G. E.; Archibong, U. D.; Ighodaro, A. Copper Nanoparticles and Their Oxides: Optical, Anticancer and Antibacterial Properties. *Int. Nano Lett.* **2022**, *12* (4), 379−398.

(24) Aishajiang, R.; Liu, Z.; Wang, T.; Zhou, L.; Yu, D. Recent Advances in Cancer Therapeutic Copper-Based Nanomaterials for Antitumor Therapy. *Molecules* **2023**, *28* (5), 2303.

(25) Tsymbal, S.; Li, G.; Agadzhanian, N.; Sun, Y.; Zhang, J.; Dukhinova, M.; Fedorov, V.; Shevtsov, M. Recent Advances in Copper-Based Organic Complexes and Nanoparticles for Tumor Theranostics. *Molecules* **2022**, *27*, 7066.

(26) Ren, D.; Cheng, Y.; Xu, W.; Qin, W.; Hao, T.; Wang, F.; Hu, Y.; Ma, L.; Zhang, C. Copper-Based Metal-Organic Framework Induces NO Generation for Synergistic Tumor Therapy and Antimetastasis Activity. *Small* **2023**, *19* (4), 2205772.

(27) Dolati, M.; Tafvizi, F.; Salehipour, M.; Komeili Movahed, T.; Jafari, P. Biogenic Copper Oxide Nanoparticles from Bacillus Coagulans Induced Reactive Oxygen Species Generation and Apoptotic and Anti-Metastatic Activities in Breast Cancer Cells. *Sci. Rep.* **2023**, *13* (1), 1−19.

(28) Wang, Y.; Yang, F.; Zhang, H. X.; Zi, X. Y.; Pan, X. H.; Chen, F.; Luo, W. D.; Li, J. X.; Zhu, H. Y.; Hu, Y. P. Cuprous Oxide Nanoparticles Inhibit the Growth and Metastasis of Melanoma by Targeting Mitochondria. *Cell Death Dis.* **2013**, *4*, e783.

(29) Spoerlein, C.; Mahal, K.; Schmidt, H.; Schobert, R. Effects of Chrysin, Apigenin, Genistein and Their Homoleptic Copper(II) Complexes on the Growth and Metastatic Potential of Cancer Cells. *J. Inorg. Biochem.* **2013**, *127*, 107−115.

(30) Shi, X.; Chen, Z.; Wang, Y.; Guo, Z.; Wang, X. Hypotoxic Copper Complexes with Potent Anti-Metastatic and Anti-Angiogenic Activities against Cancer Cells. *Dalt. Trans.* **2018**, *47* (14), 5049−5054.

(31) Guerreiro, J. F.; Gomes, M. A. G. B.; Pagliari, F.; Jansen, J.; Marafioti, M. G.; Nistico, C.; Hanley, R.; Costa, R. O.; Ferreira, S. S.; Mendes, F.; Fernandes, C.; Horn, A.; Tirinato, L.; Seco, J. Iron and Copper Complexes with Antioxidant Activity as Inhibitors of the Metastatic Potential of Glioma Cells. *RSC Adv.* **2020**, *10* (22), 12699−12710.

(32) Kalaiarasi, A.; Sankar, R.; Anusha, C.; Saravanan, K.; Aarthy, K.; Karthic, S.; Mathuram, T. lemuel; Ravikumar, V. Copper Oxide Nanoparticles Induce Anticancer Activity in A549 Lung Cancer Cells by Inhibition of Histone Deacetylase. *Biotechnol. Lett.* **2018**, *40* (2), 249−256.

(33) Ermini, M. L.; Summa, M.; Zamborlin, A.; Frusca, V.; Mapanao, A. K.; Mugnaioli, E.; Bertorelli, R.; Voliani, V. Copper Nano-Architectures Topical Cream for the Accelerated Recovery of Burnt Skin. *Nanoscale Adv.* **2023**, *5* (4), 1212−1219.

(34) Sarogni, P.; Zamborlin, A.; Mapanao, A. K.; Logghe, T.; Brancato, L.; van Zwol, E.; Menicagli, M.; Giannini, N.; Gonnelli, A.; Linsalata, S.; Colenbier, R.; Van den Bossche, J.; Paiar, F.; Bogers, J.; Voliani, V. Hyperthermia Reduces Irradiation-Induced Tumor Repopulation in an in-Vivo Pancreatic Carcinoma Model. *Adv. Biol.* **2023**, *7*, No. e2200229.

(35) Fischer, D.; Fluegen, G.; Garcia, P.; Ghaffari-Tabrizi-Wizsy, N.; Gribaldo, L.; Huang, R. Y. J.; Rasche, V.; Ribatti, D.; Rousset, X.; Pinto, M. T.; Viallet, J.; Wang, Y.; Schneider-Stock, R. The CAM Model—Q&A with Experts. *Cancers (Basel)* **2023**, *15* (1), 191.

(36) Rovithi, M.; Avan, A.; Funel, N.; Leon, L. G.; Gomez, V. E.; Wurdinger, T.; Griffioen, A. W.; Verheul, H. M. W.; Giovannetti, E. Development of Bioluminescent Chick Chorioallantoic Membrane (CAM) Models for Primary Pancreatic Cancer Cells: A Platform for Drug Testing. *Sci. Rep.* **2017**, *7*, 1−13.

(37) Livak, K. J.; Schmittgen, T. D. Analysis of Relative Gene Expression Data Using Real-Time Quantitative PCR and the 2-ΔΔCT Method. *Methods* **2001**, *25* (4), 402−408.

(38) Mapanao, A. K.; Sarogni, P.; Santi, M.; Menicagli, M.; Gonnelli, A.; Zamborlin, A.; Ermini, M. L.; Voliani, V. Pro-Apoptotic and Size-Reducing Effects of Protein Corona-Modulating Nano-Architectures Enclosing Platinum Prodrug in in Vivo Oral Carcinoma. *Biomater. Sci.* **2022**, *10* (21), 6135−6145.

(39) Santi, M.; Frusca, V.; Ermini, M. L.; Mapanao, A. K.; Sarogni, P.; Gonnelli, A.; Giannini, N.; Zamborlin, A.; Biancalana, L.; Marchetti, F.; Voliani, V. Hybrid Nano-Architectures Loaded with Metal Complexes for the Co-Chemotherapy. *J. Mater. Chem. B* **2023**, *11* (2), 325−334.

(40) Avigo, C.; Cassano, D.; Kusmic, C.; Voliani, V.; Menichetti, L. *Enhanced Photoacoustic Signal of Passion Fruit-Like Nanoarchitectures in a Biological Environment.* **2017**, *121*, 6955.

(41) Miquel, M.; Zhang, S.; Pilarsky, C. Pre-Clinical Models of Metastasis in Pancreatic Cancer. *Front. Cell Dev. Biol.* **2021**, *9*, 1.

(42) Jbara, A.; Lin, K. T.; Stossel, C.; Siegfried, Z.; Shqerat, H.; Amar-Schwartz, A.; Elyada, E.; Mogilevsky, M.; Raitses-Gurevich, M.; Johnson, J. L.; Yaron, T. M.; Ovadia, O.; Jang, G. H.; Danan-Gotthold, M.; Cantley, L. C.; Levanon, E. Y.; Gallinger, S.; Krainer, A. R.; Golan, T.; Karni, R. RBFOX2Modulates a Metastatic Signature of Alternative Splicing in Pancreatic Cancer. *Nature* **2023**, *617* (7959), 147−153.

(43) Fujimura, K.; Choi, S.; Wyse, M.; Strnadel, J.; Wright, T.; Klemke, R. Eukaryotic Translation Initiation Factor 5A (EIF5A) Regulates Pancreatic Cancer Metastasis by Modulating RhoA and Rho-Associated Kinase (ROCK) Protein Expression Levels. *J. Biol. Chem.* **2015**, *290* (50), 29907−29919.

(44) Wang, Z.; Jiang, J.; Qin, T.; Xiao, Y.; Han, L. EIF5A Regulates Proliferation and Chemoresistance in Pancreatic Cancer through the SHH Signalling. *Pathway. J. Cell. Mol. Med.* **2019**, *23* (4), 2678−2688.

(45) Ayres Pereira, M.; Chio, I. I. C. Metastasis in Pancreatic Ductal Adenocarcinoma: Current Standing and Methodologies. *Genes (Basel)* **2020**, *11*, 6.

(46) Bloise, N.; Strada, S.; Dacarro, G.; Visai, L. Gold Nanoparticles Contact with Cancer Cell: A Brief Update. *Int. J. Mol. Sci.* **2022**, *23* (14), 7683.

(47) Balamurugan, K.; Schaffner, W. Copper Homeostasis in Eukaryotes: Teetering on a Tightrope. *Biochim. Biophys. Acta* **2006**, *1763* (7), 737−746.

(48) Nishioka, R.; Itoh, S.; Gui, T.; Gai, Z.; Oikawa, K.; Kawai, M.; Tani, M.; Yamaue, H.; Muragaki, Y. SNAIL Induces Epithelial-to-Mesenchymal Transition in a Human Pancreatic Cancer Cell Line (BxPC3) and Promotes Distant Metastasis and Invasiveness in Vivo. *Exp. Mol. Pathol.* **2010**, *89* (2), 149−157.

(49) Haraguchi, M. The Role of the Transcriptional Regulator Snail in Cell Detachment, Reattachment and Migration. *Cell Adhes. Migr.* **2009**, *3* (3), 259−263.

(50) Yang, J.; Mani, S. A.; Weinberg, R. A. Exploring a New Twist on Tumor Metastasis. *Cancer Res.* **2006**, *66* (9), 4549−4552.

(51) Palaniappan, T. K.; Šlekienė, L.; Jonasson, A. K.; Gilthorpe, J.; Gunhaga, L. CAM-Delam: An in Vivo Approach to Visualize and Quantify the Delamination and Invasion Capacity of Human Cancer Cells. *Sci. Rep.* **2020**, *10* (1), 1−11.

(52) Sudha, T.; Yalcin, M.; Lin, H.-Y.; Elmetwally, A. M.; Nazeer, T.; Arumugam, T.; Phillips, P.; Mousa, S. A. Suppression of Pancreatic Cancer by Sulfated Non-Anticoagulant Low Molecular Weight Heparin. *Cancer Lett.* **2014**, *350* (1−2), 25−33.

(53) Zhao, Z.; Bauer, N.; Aleksandrowicz, E.; Yin, L.; Gladkich, J.; Gross, W.; Kaiser, J.; Hackert, T.; Strobel, O.; Herr, I. Intraductal Papillary Mucinous Neoplasm of the Pancreas Rapidly Xenografts in Chicken Eggs and Predicts Aggressiveness. *Int. J. Cancer* **2018**, *142* (7), 1440−1452.

(54) Gharibi, A.; La Kim, S.; Molnar, J.; Brambilla, D.; Adamian, Y.; Hoover, M.; Hong, J.; Lin, J.; Wolfenden, L.; Kelber, J. A. Is a Pre-Malignant Biomarker That Promotes Therapy Resistance and Metastatic Potential in Pancreatic Cancer. *Sci. Rep.* **2017**, *7* (1), 1−14.

(55) Augoff, K.; Hryniewicz-Jankowska, A.; Tabola, R.; Stach, K. MMP9: A Tough Target for Targeted Therapy for Cancer. *Cancers (Basel)* **2022**, *14* (7), 1847.

(56) von Burstin, J.; Eser, S.; Paul, M. C.; Seidler, B.; Brandl, M.; Messer, M.; von Werder, A.; Schmidt, A.; Mages, J.; Pagel, P.; Schnieke, A.; Schmid, R. M.; Schneider, G.; Saur, D. E-Cadherin Regulates Metastasis of Pancreatic Cancer In Vivo and Is Suppressed by a SNAIL/HDAC1/HDAC2 Repressor Complex. *Gastroenterology* **2009**, *137* (1), 361−371.E5.

(57) Turski, M. L.; Thiele, D. J. New Roles for Copper Metabolism in Cell Proliferation, Signaling, and Disease. *J. Biol. Chem.* **2009**, *284* (2), 717−721.

(58) Batzer, M. A.; Deininger, P. L. Alu Repeats and Human Genomic Diversity. *Nat. Rev. Genet.* **2002**, *3* (5), 370−379.

(59) Deryugina, E. I.; Quigley, J. P. Chick Embryo Chorioallantoic Membrane Model Systems to Study and Visualize Human Tumor Cell Metastasis. *Histochem. Cell Biol.* **2008**, *130* (6), 1119−1130.